J. Fluid Mech. (1983), *vol.* 128, *pp.* 1–20
Printed in Great Britain

Hydromagnetic waves in a differentially rotating sphere

By D. R. FEARN AND M. R. E. PROCTOR
Department of Applied Mathematics and Theoretical Physics,
Silver Street, Cambridge CB3 9EW

(Received 28 May 1982 and in revised form 9 November 1982)

The linear stability of a uniformly internally heated, self-gravitating, rapidly rotating fluid sphere is investigated in the presence of an azimuthal magnetic field $B_0(r, \theta)\hat{\boldsymbol{\phi}}$ and azimuthal shear flow $U_0(r, \theta)\hat{\boldsymbol{\phi}}$ (where (r, θ, ϕ) are spherical polar coordinates). Solutions are calculated numerically for magnetic field strengths that produce a Lorentz force comparable in magnitude to that of the Coriolis force. The critical Rayleigh number R_c is found to reach a minimum here and the qualitative behaviour of the thermally driven instabilities in the absence of a shear flow ($U_0 = 0$) is similar to that found by earlier workers (e.g. Fearn 1979*b*) for the simpler basic state $B_0 = r \sin \theta$. The effect of a shear flow is followed as its strength (measured by the magnetic Reynolds number R_m) is increased from zero. In the case where the ratio q of thermal to magnetic diffusivities is small ($q \ll 1$) the effect of the flow becomes significant when $R_m = O(q)$. For $R_m > q$ three features are evident as R_m is increased: the perturbation in the temperature field (but not the other variables when $R_m < O(1)$) becomes increasingly localized at some point (r_L, θ_L); the phase speed of the instability tends towards the fluid velocity at that point; and R_c increases with R_m with the suggestion that $R_c \propto R_m/q$ for $R_m \gg q$ although the numerical resolution is insufficient to verify this. Greater resolution is achieved for a simpler problem which retains the essential physics and is described in the accompanying paper (Fearn & Proctor 1983). The possible significance of these results to the geomagnetic secular variation is discussed.

1. Introduction

It is generally accepted that the Earth's magnetic field has been maintained over geological time by the interaction of the magnetic and velocity fields in the molten outer core (see e.g. Moffatt 1978). This so-called dynamo process converts the kinetic energy of the fluid into magnetic energy, balancing the losses due to ohmic decay. Current thought favours buoyancy as the cause of the fluid motions; light material which is released at the inner-core boundary as the Earth cools and the inner core freezes being the most likely source of the buoyancy (see e.g. Gubbins, Masters & Jacobs 1979; Loper & Roberts 1983). An understanding of the behaviour of the Earth's magnetic field thus requires a study of convection in a rapidly rotating system in the presence of a magnetic field. The full hydromagnetic dynamo problem involves the simultaneous solution of the Navier–Stokes equation and the magnetic induction equation, which together form a complicated nonlinear system. Most progress in understanding the dynamo mechanism has been made by studying the simpler kinematic dynamo problem, which solves only the induction equation for a given velocity field $\mathbf{U}$, and neglects the back reaction of the magnetic field $\mathbf{B}$ on the flow (see Moffatt 1978). Another approach to gaining some understanding of the behaviour of the Earth's field has been to neglect the need for the maintenance of the field and

look at the linear stability of some basic state $\mathbf{B}_0$, $\mathbf{U}_0$. Such studies have led to the discovery of a large number of different mechanisms for instability; buoyancy or magnetically driven, diffusive or non-diffusive, and on all possible timescales from inertial to thermal diffusion. Reviews have been made by Acheson & Hide (1973), Acheson (1978*a*), Roberts (1978) and Eltayeb (1981).

The first studies of the onset of convection in rapidly rotating magnetic systems used a plane layer geometry (Bénard layer) and a uniform magnetic field. Perhaps the most important result of this work was that, although, individually, rotation and magnetic fields inhibit convection, adding a magnetic field to a rapidly rotating system can counteract the geostrophic constraint and facilitiate convection (see Chandrasekhar 1961; Eltayeb & Roberts 1970; Elyayeb 1972, 1975). The critical Rayleigh number R_c falls as the magnetic field strength (as measured by the parameter Λ defined in (2.5)) increases until the Lorentz force has grown to balance the Coriolis force ($\Lambda = O(1)$). At higher field strengths the magnetic field reverts to its more familiar role of inhibiting convection and R_c increases with Λ. Thus convection is most easily driven when $\Lambda = O(1)$, and it has been suggested that perhaps it is in this parameter range that the geodynamo would operate most efficiently (see e.g. Soward 1979*a*).

A plane layer with a uniform magnetic field is not a very realistic model for the Earth's core, but a spherical geometry is difficult to work with. Intermediate models have been studied by Acheson (1973, 1978*a*) (cylindrical geometry) and Soward (1979*b*) (plane layer), who both consider a toroidal magnetic field $\mathbf{B}_0 = B_0(s)\hat{\boldsymbol{\phi}}$, where s is the distance from the rotation axis. Such studies retain a certain amount of mathematical simplicity, while the cylindrical magnetic-field geometry is rather closer to the geomagnetic field. Much effort has been made to identify the travelling-wave instabilities of such systems with the geomagnetic secular variation (GSV) and perhaps too much emphasis has been placed on finding waves that show a preference for westward propagation. No satisfactory explanation of the GSV has yet been achieved.

The principal aim of the linear stability studies has been as a complement to the kinematic dynamo problem, to investigate how the presence of a magnetic field influences the convective motions which are thought to generate the field. For this purpose it has been argued that the precise form of the field is unimportant and the field that is, mathematically, the easiest to work with ($\mathbf{B}_0 = B_M s\hat{\boldsymbol{\phi}}$) has generally been chosen (see Malkus 1967; Eltayeb & Kumar 1977; Roberts & Loper 1979; Soward 1979*b*; Fearn 1979*a*, *b*). This claim seems to be quite tenable since studies with this field give results qualitatively similar to those obtained with a uniform field; thermal instabilities being most easily driven when $\Lambda = O(1)$. Indeed, the results of this paper which are for $\mathbf{B}_0 = B_0(r, \theta)\hat{\boldsymbol{\phi}}$ (where (r, θ, ϕ) are spherical polar coordinates) confirm this. However, the choice of the basic state is important because the magnetic field can itself be unstable when $\Lambda \geqslant O(1)$. Many different instability mechanisms have been discovered (see Roberts & Loper 1979; Soward 1979*b*; Fearn 1979*b*) and these have considerably complicated the stability picture. It has therefore become necessary to investigate the conditions under which the magnetic field becomes unstable. Almost all the work to date has ben concerned with the one field ($\mathbf{B}_0 = B_M s\hat{\boldsymbol{\phi}}$) so no general rules for the stability of other fields can be predicted. Some progress has been made by Acheson (1973, 1978*a*, 1982) using a local analysis for basic states of the form

$$\mathbf{B}_0 = B_0(s)\hat{\boldsymbol{\phi}}, \quad \mathbf{U}_0 = U_0(s)\hat{\boldsymbol{\phi}}, \tag{1.1}$$

and his predictions for the existence of field gradient and buoyancy-catalysed

instabilities are consistent with the global results for the field $\mathbf{B}_0 = B_M s\hat{\boldsymbol{\phi}}$ (Fearn 1979*b*). An extension of the local analysis to the more general basic state

$$\mathbf{B}_0 = B_0(s,z)\hat{\boldsymbol{\phi}}, \quad \mathbf{U}_0 = U_0(s,z)\hat{\boldsymbol{\phi}} \tag{1.2}$$

(where $z = r\cos\theta$ is the coordinate in the direction of the rotation axis) is discussed in appendix A (see also Acheson 1978*b*). Generalized forms (A 11) and (A 15) of Acheson's stability criteria are found and these predict that z-structure is destabilizing. To date, no global results exist to complement this local analysis.

The subject is thus at a stage where the linear stability of the basic state

$$\mathbf{B}_0 = B_0(r,\theta)\hat{\boldsymbol{\phi}}, \quad \mathbf{U}_0 = U_0(r,\theta)\hat{\boldsymbol{\phi}}$$

needs to be tackled. There are several reasons for this. Magnetic fields $B_0(s)\hat{\boldsymbol{\phi}}$ are special in that no flow $\mathbf{U}_0$ is required for the basic state to be in equilibrium (see e.g. Braginsky 1980). Only the field $B_0 \propto s$ has been studied in detail and we only have Acheson's local analysis to give us some indication of how typical this field is. The effect of the sheared flow $\mathbf{U}_0$ has been largely neglected (primarily because of the added complexity it adds to the analysis), but, since geostrophic flows are easily set up in rapidly rotating systems and since a basic state with $\mathbf{B}_0 = B_0(r,\theta)$ requires a non-zero $\mathbf{U}_0(r,\theta)$ for equilibrium (see Braginsky 1980), a differential rotation is almost certainly present in the core and is likely to play an important role. Indeed it is believed that a strong azimuthal flow is responsible for stretching out poloidal field lines to produce a large toroidal field (see Moffatt 1978).

In this paper we describe the first results of a study of the linear stability of the basic state $B_0(r,\theta)\hat{\boldsymbol{\phi}}$, $U_0(r,\theta)\hat{\boldsymbol{\phi}}$ in a spherical geometry. The effects of buoyancy are included but we do not consider compositional buoyancy. Instead, because it is easier to work with, thermal buoyancy is used and the hope is that qualitatively the results will be similar. Another reason for using thermal buoyancy is that results are available for the case $B_0 \propto s$ and they provide a very necessary check for the numerical calculations of this paper. The details of the model are given in §2, and some discussion of the numerical method of solution is given in appendix B. Results were computed for field strengths in the range $\Lambda = O(1)$, and these are discussed in §3. First, results for the field $B_0 \propto s$ are found, and these are in agreement with those of Fearn (1979*b*), which involved a completely independent formulation of the problem. Next the field $\mathbf{B}_0 = B_M 8r^2(1-r^2)\sin\theta\cos\theta\hat{\boldsymbol{\phi}}$ is investigated. We concentrate our attention on the thermally driven modes and find that qualitatively they behave in much the same way as for the field $\mathbf{B}_0 = B_M s\hat{\boldsymbol{\phi}}$; the critical Rayleigh number reaches a minimum when $\Lambda = O(1)$ (see figure 2 and also Eltayeb & Kumar 1977; Fearn 1979*b*). Magnetically driven modes are also present, and although an exhaustive investigation was not carried out we found both the buoyancy-catalysed instabilities and the field-gradient instabilities (see Acheson 1978*a*; Fearn 1979*b*) to be present.

The most interesting results of the present study were found when investigating the effect of including an azimuthal flow $U_0(r,\theta)\hat{\boldsymbol{\phi}}$ in the basic state. We proceeded by fixing the form of U_0 and gradually increasing its strength (as measured by the magnetic Reynolds number R_m). We fixed the ratio q of the thermal to magnetic diffusivities to be small ($q = 10^{-6}$) and found the effects of the shear to become important when $R_m = O(q)$. In the range $q \ll R_m \ll 1$ the critical Rayleigh number R_c increases with R_m, the temperature perturbation becomes increasingly localized at some point (r_L, θ_L), and the phase speed of the wave approaches the speed of the shear flow at that point. These results are described in detail in §3 and are discussed further in §4, where we speculate on what significance they may have for the geomagnetic secular variation.

2. Governing equations and method of solution

An electrically conducting, self-gravitating fluid is contained in a rigid, electrically insulating spherical container of radius r_0, and the whole system is rotating with angular velocity $\boldsymbol{\Omega}_0 = \Omega_0 \hat{\mathbf{z}}$. The fluid is internally heated by some distribution H of heat sources and the container is taken to be a perfect thermal conductor. In the rotating frame of reference the equations describing the fluid velocity $\mathbf{U}$, the magnetic field $\mathbf{B}$ and the temperature T are, in the Boussinesq approximation

$$\left.\begin{aligned} &\frac{\partial \mathbf{U}}{\partial t} + (\mathbf{U}\cdot\nabla)\mathbf{U} + 2\boldsymbol{\Omega}_0 \times \mathbf{U} = -\nabla p + \nu\nabla^2\mathbf{U} + (\nabla\times\mathbf{B})\times\mathbf{B}/\mu\rho_0 + \frac{\mathbf{g}\rho}{\rho_0}, \\ &\frac{\partial \mathbf{B}}{\partial t} = \nabla\times(\mathbf{U}\times\mathbf{B}) + \eta\nabla^2\mathbf{B}, \\ &\frac{\partial T}{\partial t} + (\mathbf{U}\cdot\nabla)T = \kappa\nabla^2 T + H, \\ &\nabla\cdot\mathbf{U} = \nabla\cdot\mathbf{B} = 0, \end{aligned}\right\} \tag{2.1}$$

where $\mathbf{g} = -g_0\mathbf{r}/r_0$ is the gravitational acceleration and μ, ρ_0, ν, κ and η denote the magnetic permeability, mean fluid density, kinematic viscosity, thermal diffusivity and magnetic diffusivity, all of which are assumed to be constant. To complete the system (2.1) an equation of state is required. We shall use

$$\rho = \rho_0(1-\alpha(T-T_0)), \tag{2.2}$$

where ρ is the fluid density, T_0 is a mean temperature and α is the volume expansion coefficient. A linear stability analysis of (2.1) yields the equations

$$E_\eta\left(\frac{\partial \mathbf{u}}{\partial t} + R_\mathrm{m}[(\mathbf{u}\cdot\nabla)\mathbf{U}_0 + (\mathbf{U}_0\cdot\nabla)\mathbf{u}] - p_\mathrm{m}\nabla^2\mathbf{u}\right) + \hat{\mathbf{z}}\times\mathbf{u}$$
$$= -\nabla p + \Lambda[(\nabla\times\mathbf{B}_0)\times\mathbf{b} + (\nabla\times\mathbf{b})\times\mathbf{B}_0] + qR\vartheta\mathbf{r}, \tag{2.3a}$$

$$\frac{\partial \mathbf{b}}{\partial t} = \nabla\times(\mathbf{u}\times\mathbf{B}_0) + R_\mathrm{m}\nabla\times(\mathbf{U}_0\times\mathbf{b}) + \nabla^2\mathbf{b}, \tag{2.3b}$$

$$\frac{\partial \vartheta}{\partial t} + (\mathbf{u}\cdot\nabla)T_0 + R_\mathrm{m}(\mathbf{U}_0\cdot\nabla)\vartheta = q\nabla^2\vartheta, \tag{2.3c}$$

$$\nabla\cdot\mathbf{u} = \nabla\cdot\mathbf{b} = 0, \tag{2.3d,e}$$

where the basic (unperturbed) magnetic, velocity and temperature fields are

$$\mathbf{B}_0 = B_0(r,\theta)\hat{\boldsymbol{\phi}}, \quad \mathbf{U}_0 = U_0(r,\theta)\hat{\boldsymbol{\phi}}, \quad T_0 = T_0(r,\theta), \tag{2.4}$$

and $\mathbf{b}$, $\mathbf{u}$ and ϑ are the perturbations of this basic state. The mean field variables $\mathbf{B}_0$, $\mathbf{U}_0$ and T_0 have been normalized using $B_\mathrm{M} = \max|B_0|$, $U_\mathrm{M} = \max|U_0|$ and βr_0, where $\beta = \max|\nabla T_0|$. The perturbation variables have been non-dimensionalized on the magnetic diffusion timescale $\tau_\eta = r_0^2/\eta$, lengthscale r_0, temperature βr_0, magnetic field strength B_M and velocity η/r_0. The dimensionless parameters used in (2.3) are a modified Ekman number E_η, magnetic Reynolds number R_m, magnetic Prandtl number p_m, magnetic field strength Λ, diffusivity ratio q, and modified Rayleigh number R, defined by

$$\left.\begin{aligned} &R = \frac{g\alpha\beta r_0^2}{2\Omega_0\kappa}, \quad \Lambda = \frac{B_\mathrm{M}^2}{2\Omega_0\mu\rho_0\eta}, \quad E_\eta = \frac{\eta}{2\Omega_0 r_0^2}, \\ &R_\mathrm{m} = \frac{U_\mathrm{M} r_0}{\eta}, \quad p_\mathrm{m} = \frac{\nu}{\eta}, \quad q = \frac{\kappa}{\eta}. \end{aligned}\right\} \tag{2.5}$$

Before tackling a solution of (2.3), one simplification will be made. The Ekman number is very small ($E_\eta = O(10^{-9}) \ll 1$) and experience with this problem (see Eltayeb & Kumar 1977; Fearn 1979*a*, *b*) has shown that, except when the magnetic field strength is very small ($\Lambda \leqslant O(E_\eta)$), inertial terms in the momentum equation are unimportant when looking for the onset of convection. In this paper we shall be restricting our attention to $\Lambda = O(1)$, and consequently the term in (2.3) multiplied by E_η will be neglected. The remaining terms in (2.3) form an eighth-order system, which we will solve subject to the boundary conditions

$$\left.\begin{aligned} \mathbf{u}.\hat{\mathbf{r}} = 0, \quad \vartheta = 0, \quad \mathbf{b} = \mathbf{b}^{\mathrm{ex}} \quad (r = 1), \\ \mathbf{u} = \mathbf{b} = \vartheta = 0 \quad (r = 0), \end{aligned}\right\} \tag{2.6}$$

where $\mathbf{b}^{\mathrm{ex}}$ is an external potential field.

The problem (2.3) with (2.6) is separable in ϕ and t, so we shall make the modal expansion

$$[\mathbf{u}, \mathbf{b}, p, \vartheta] = [\mathbf{u}(r,\theta), \mathbf{b}(r,\theta), p(r,\theta), \vartheta(r,\theta)]\, e^{pt}\, e^{im\phi}. \tag{2.7}$$

We are now left with a two-dimensional partial differential equation in r and θ. The problem is not further separable, but in the special case $B_0 = s$, $U_0 = 0$ it was found useful to expand the variables in spherical harmonics (see Eltayeb & Kumar 1977; Fearn 1979*b*). The advantage of this approach depended on the fact that the basic field B_0 appears in the form $F = B_0/s$ in the governing equations. When $B_0 = s$, $F = 1$, which provides a very great simplification and is the reason why the field $B_0 = s$ has received so much attention. We wish to study the more general basic state (2.4), so we have decided not to try an expansion in spherical harmonics but to solve the system (2.3)–(2.6) directly by using finite differences with N grid points in the r-direction and L in the θ-direction. The resulting matrix eigenvalue problem was solved using two different numerical methods; the LR algorithm, which finds all the eigenvalues but is severely limited in resolution, and inverse iteration (II) which is capable of much better resolution but finds only one eigenvalue. Details of the numerical scheme are given in appendix B.

The procedure that we adopted to find the results discussed in §3 was first to use LR with $N = L = 8$ to generate most of the data. Then, at selected points in the (Λ, m) parameter space, II was used with $N = L = 8$, 10, 15 and 20 to find how well the solution converged. The II method provides the eigenfunction as well as the eigenvalue, and we drew contour plots of the dependent variables b_r, b_θ, u_r, u_θ and ϑ. The smoothness of the eigenfunction gives some indication of the convergence, and comparison of the eigenfunctions at different truncation levels ensures that it is the same mode that is being looked at for the different values of N, L.

3. Numerical results

Before calculating a numerical solution, $B_0(r,\theta)$, $U_0(r,\theta)$ and $T_0(r,\theta)$ must be specified, together with the parameters Λ, R_{m}, q and the azimuthal wavenumber m. Clearly it is only possible to explore a very restricted part of this parameter space and we have chosen in this paper to look mainly at $m = 1, 2$ and $q = 10^{-6}$ (since this is approximately the molecular diffusivity ratio for the Earth and should be typical of the limit $q \ll 1$). The basic temperature profile was chosen to be that due to a uniform distribution of heat sources ($T_0 = -\frac{1}{2}r^2$) since this was used by most other authors who have studied convection in a sphere (see Roberts 1968; Soward 1977; Eltayeb & Kumar 1977; Fearn 1979*a*, *b*). This choice facilitates comparisons with

previous work and it provides a typical unstable temperature gradient throughout the sphere. There may be a case for studying other density distributions; in particular there is interest in convection in a core which is unstably stratified near the inner-core boundary but stably stratified near the mantle–core boundary (see e.g. Whaler 1980; Fearn & Loper 1981), but that we leave for future study.

The results that we describe in this paper fall into three groups: (*a*) $B_0 = s = r\sin\theta$, $U_0 = 0$; (*b*) $B_0 = 8r^2(1-r^2)\sin\theta\cos\theta$, $U_0 = 0$; and (*c*) $B_0 = 8r^2(1-r^2)\sin\theta\cos\theta$, $U_0 = 64r^3(1-r^2)^2\sin\theta\cos^2\theta$ or $U_0 = -\frac{25}{16}\sqrt{5}\,r(1-r^2)^2\sin\theta$. The first case was used to show that the results from this program agreed with earlier work (Fearn 1979*b*), the second case to investigate how the choice of basic magnetic field affects the stability diagram, and finally case (*c*) enabled the role of differential rotation to be studied. The precise choice of the fields B_0 and U_0 will be discussed in each subsection.

(*a*) *Checking case*

The algebra involved in deriving the discretized equations gives considerable scope for error. It is therefore crucial to make some checks before proceeding to generate results for cases not previously studied. The *LR* and II methods were programmed mostly independently and their results were found to be in exact agreement for all basic states B_0, U_0 investigated, thus providing a useful check on much of the coding. The basic state

$$B_0 = s, \quad U_0 = 0 \tag{3.1}$$

has been investigated in the spherical geometry by Eltayeb & Kumar (1977) and by Fearn (1979*b*). The qualitative behaviour found in these two papers was the same but there was not exact numerical agreement (see Fearn 1979*b*). This may have been because Eltayeb & Kumar failed to find the minimum critical Rayleigh number. It was decided to insert the basic state (3.1) into the numerical scheme described in §2 and try to reproduce the results of Fearn (1979*b*). Precise agreement cannot be expected since we have used a finite-difference approximation in the θ-direction while Fearn used a spherical harmonic expansion. The case we chose to compare was $\Lambda = 0{\cdot}5$, $m = 2$. The results given in table 1 of Fearn (1979*b*) are for $q = 0$, but we recalculated them for $q = 10^{-6}$ and found the answers to be the same to five or six significant figures. Perhaps the closest check available is to compare the results from Fearn (1979*b*) for 10 spherical harmonics and 21 radial grid points,

$$R_c = 113{\cdot}3, \quad \omega_c = 42{\cdot}35, \tag{3.2}$$

with the results obtained here for $N = L = 20$,

$$R_c = 115{\cdot}0, \quad \omega_c = 43{\cdot}25, \tag{3.3}$$

where R_c is the critical Rayleigh number ($\mathrm{Re}\,(p) = 0$) and ω_c is the corresponding frequency ($\omega = -\mathrm{Im}\,(p)$) quoted in units of the thermal diffusion timescale. The expected error in (3.2) and (3.3) is $O(h^2)$, i.e. $O(0{\cdot}25\,\%)$. The errors in R_c and ω_c are respectively about 6 and 8 times this, which does not seem unreasonable. A further comparison can be made if we assume that we can write

$$R_c^L = R_c^\infty + \frac{\epsilon_1}{L^2} + \frac{\epsilon_2}{L^4} + O\left(\frac{1}{L^6}\right). \tag{3.4}$$

Ignoring the $O(1/L^6)$ term, ϵ_1 and ϵ_2 can be calculated given values of R_c at three different truncations and then an estimate of the value R_c^∞ can be obtained. There is little difference between 10 and 12 spherical harmonics, so Fearn 1979*b*) gives

$$R_c^\infty = 115{\cdot}6, \quad \omega_c^\infty = 43{\cdot}30, \tag{3.5}$$

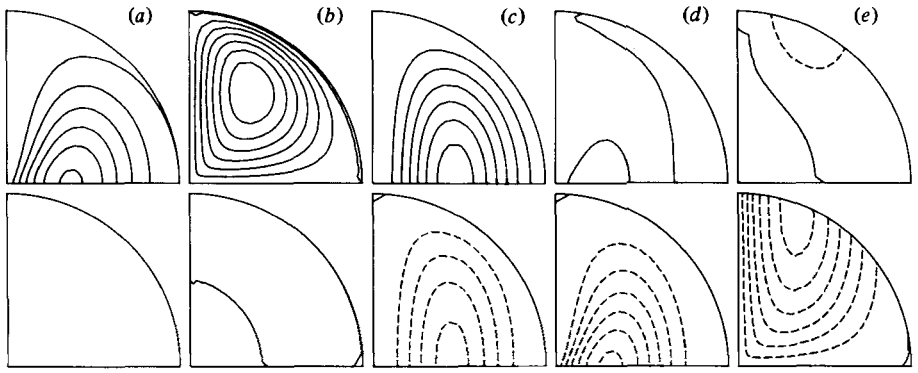

FIGURE 1. The solution for the marginally stable mode is illustrated by contour plots of (from left to right) (*a*) b_r, (*b*) b_θ, (*c*) $q\vartheta$, (*d*) u_r, and (*e*) u_θ in the quadrant $0 < r < 1, 0 < \theta < \frac{1}{2}\pi$. Both real (upper) and imaginary (lower) parts are shown, and the contour intervals have been chosen the same for both parts. The zero and positive contours are drawn with a full line, the negative contours with a broken line. All eigenfunctions with dipole (quadrupole) parity have been normalized to make the value of b_θ (b_r) at $r = 1, \theta = \frac{1}{2}\pi$ equal to unity. This example is for basic state (3.1) with $\Lambda = 0{\cdot}5$, $m = 2$, $q = 10^{-6}$, quadrupole parity and truncation $N = L = 20$, which gives $R_c = 115{\cdot}0$, $\omega_c = 43{\cdot}25q$. The eigenfunction is qualitatively the same for other values of N and L. The contour intervals are (*a*) 1·0, (*b*) 1·0, (*c*) 1·0, (*d*) 20 and (*e*) 30.

and with $N = L$ taking values 11, 16 and 20 the present method gives

$$R_c^\infty = 115{\cdot}4, \quad \omega_c = 43{\cdot}14. \tag{3.6}$$

The agreement is not precise but is very close – to within less than 0·2 % and 0·4 % respectively for R_c and ω_c. We feel this is as good as can be expected and that this provides a check both for the present work and for that of Fearn (1979*b*), which was formulated completely independently.

For comparison with the results of §3(*b*), (*c*), the eigenfunction corresponding to the solution (3.3) is shown in figure 1.

(*b*) *More realistic field*

Once satisfied that our program was producing sensible results we proceeded to explore new ground. We first focused our attention on the role that the choice of the basic magnetic field B_0 plays in determining the stability of our system. As has already been mentioned, the field $B_0 = s$ has been extensively studied because of its simplicity. Here we look at a field that is much more representative of the Earth's toroidal field:

$$B_0 = 8r^2(1-r^2)\sin\theta\cos\theta. \tag{3.7}$$

(The factor 8 appears because we have normalized B_0 to have a maximum value of unity.) The field (3.7) has the property that it vanishes on the mantle–core boundary ($r = 1$), this being required since the mantle is a good electrical insulator. Also B_0 takes opposite signs in the northern and southern hemispheres as we expect for a toroidal field stretched out by differential rotation from a weak poloidal field. It should be emphasized here that the study of the field (3.7) with shear flow $U_0 = 0$ is somewhat unrealistic, but nevertheless we feel it is justified as a step along the way to understanding the stability of basic states of the form $B_0(s, z)$, $U_0(s, z)$. The case where $B_0 = B_0(s)$ only is special in that when B_0 depends on z a steady basic state cannot

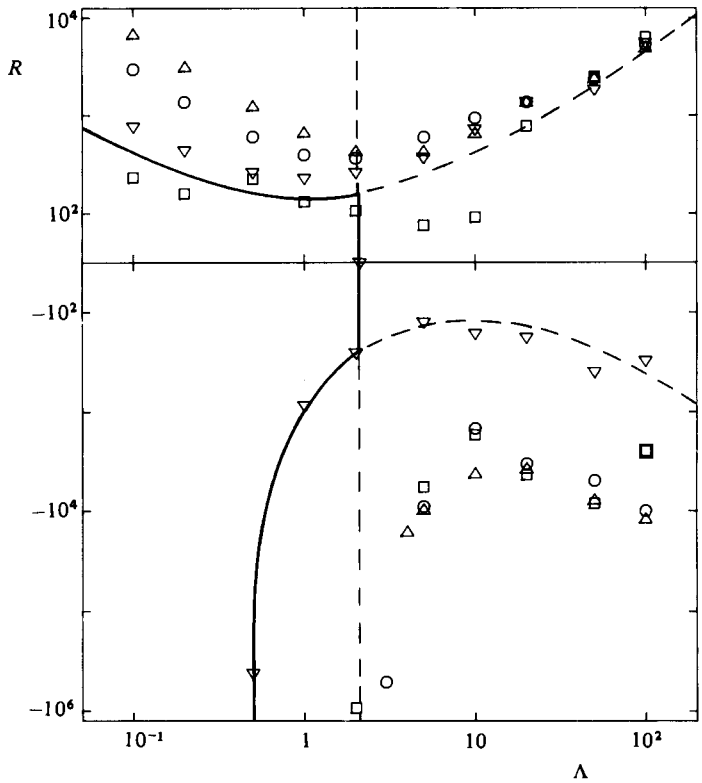

FIGURE 2. The stability diagram for the field (3.7) with $q = 10^{-6}$. The data points plotted were obtained using the LR method with $N = L = 8$, and the convergence checked in selected cases using II. Convergence was not always good, so the exact location of the stability boundary and the identity of the preferred mode are uncertain. Nevertheless we believe the qualitative picture to be correct. The diffusive thermal instability behaves much as it does for field (3.1) (see Fearn 1979*b*, figure 1). The buoyancy-catalysed instability is present. The modes illustrated are ▽, $m = 1$, dipole; △, $m = 1$, quadrupole; □, $m = 2$, dipole and ○, $m = 2$, quadrupole. Some of the data points do not fit well onto smooth curves. This may in part be due to errors caused by lack of resolution, but it may also be a real effect as the most-unstable mode switches from one mode to another (cf. Fearn 1979*b*). A rough stability boundary is shown, with the region to the right of the full line being unstable to one or more of the modes present (diffusive thermal, buoyancy-catalysed, or field gradient).

exist without a balancing shear flow given by

$$\frac{\partial}{\partial z}(\Lambda F^2 - R_m \Omega) = 0, \tag{3.8}$$

where

$$F = \frac{B_0}{s}, \quad \Omega = \frac{U_0}{s} \tag{3.9}$$

(see e.g. Braginsky 1980). Thus it might seem meaningless to look at the stability of (3.7) without incorporating the corresponding shear flow. However, in a practical situation, there are several other effects which give rise to a differential rotation which may be expressed as

$$\Omega = \Omega_B + \Omega_T + \Omega_G + \Omega_R, \tag{3.10}$$

where $\Omega_B = \Lambda F^2/R_m$, Ω_T is the thermal wind required when the body force and the

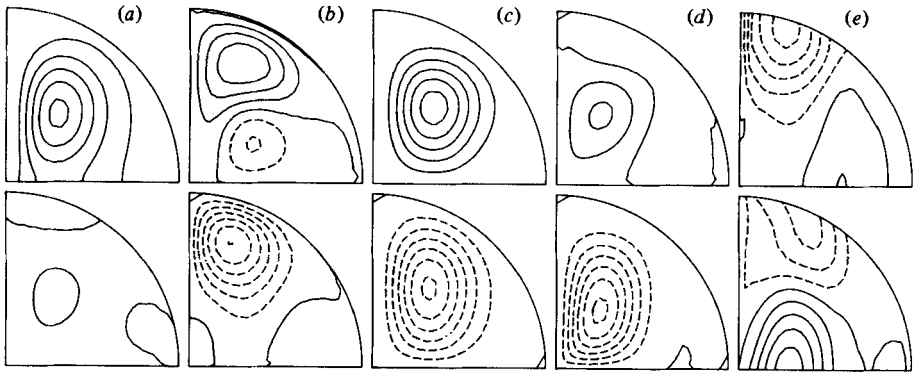

FIGURE 3. As figure 1 but for the field (3.7), $\Lambda = 1$, $m = 2$, $q = 10^{-6}$, quadrupole parity and $N = L = 20$, giving $R_c = 319{\cdot}3$, $\omega_c = 36{\cdot}54q$. The contour intervals are (*a*) 3·0, (*b*) 3·0, (*c*) 0·2, (*d*) 50, (*e*) 100.

density gradient are not aligned, $\mathbf{\Omega}_G(s)$ is an arbitrary geostrophic flow (a constant of the integration of (3.8)), and $\mathbf{\Omega}_R$ denotes the rest, which includes nonlinear effects. These can drive differential rotation of various forms depending on the curvature of the container, and the distribution of the temperature gradient (Busse & Hood 1982). It is not possible to incorporate the full $\mathbf{\Omega}$ given by (3.10) into our model, and, even if it were, it is probable that the role that differential rotation plays would be inextricably mixed up with the other effects present. Moreover, it is not clear what to choose for $\mathbf{\Omega}_G$, so it seems sensible to treat $\mathbf{\Omega}$ as a function that can be chosen independently. Obviously some physical realism is lost but this approach does enable us to isolate and, we hope, to understand the role of differential rotation in the hydromagnetic stability of rapidly rotating systems.

The results for the field (3.7) are shown in figure 2, which may be compared with figure 1 of Fearn (1979*b*). It is possible to identify three modes of instability. First there are the thermally driven instabilities, which exist only for $R > 0$. Their behaviour is much the same as was found by Fearn (1979*b*) for the field (3.1) with the critical Rayleigh number R_c reaching a minimum $O(100)$ at $\Lambda = O(1)$. At smaller field strengths ($\Lambda < O(1)$) the magnetic field acts to balance out the Coriolis force, and an increasing field facilitates convection. At higher field strengths ($\Lambda > O(1)$) the role of the magnetic field is to inhibit thermal convection. The form of the basic field B_0 thus seems not be important as far as thermal instabilities are concerned since (3.1) and (3.7) give similar results. A typical eigenfunction is illustrated in figure 3, and the convergence behaviour is shown in figure 4.

The second mode of instability that can be identified is the buoyancy-catalysed instability first studied by Roberts & Loper (1979) and Soward (1979*b*) (see also Fearn 1979*b*; Acheson 1980, 1982). This mode operates on the thermal diffusion timescale (like the thermal instabilities described above) and requires the presence of some stratification before it can become unstable. However, this stratification may be either 'stable' or 'unstable' in the thermal-instability sense and it is therefore the magnetic field which is the source of the energy that drives this instability. The presence of the stratification gives the system some extra degrees of freedom not available when $R = 0$, which enables the magnetic energy to be released. In the case of the field (3.1), only the $m = 1$ mode was found to be unstable (Loper & Roberts 1979; Soward 1979*b*; Fearn 1979*b*). This was in accordance with the local analysis by Acheson (1982) for fields $B_0 = B_0(s)$, which predicted instability for all

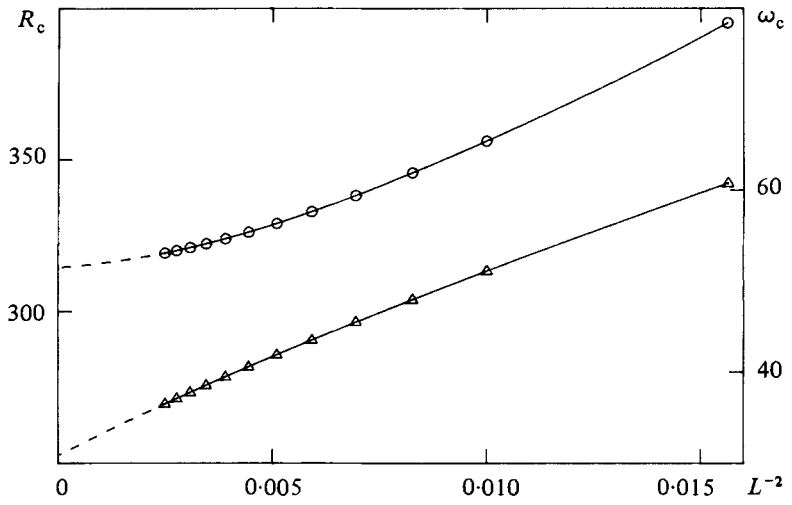

FIGURE 4. The manner in which the mode illustrated in figure 3 converges as the truncation is increased. Here $N = L$ and R_c (upper curve) and ω_c (lower curve) are plotted against $1/L^2$. The behaviour can be represented by a relation of the form (3.4), and the eigenfunction is qualitatively the same for all L. Thus although the numerical scheme gives results that are quantitatively in error, we expect to gain some correct qualitative information even at the $N = L = 8$ truncation level. The broken line shows the extrapolation to large N, L using (3.4).

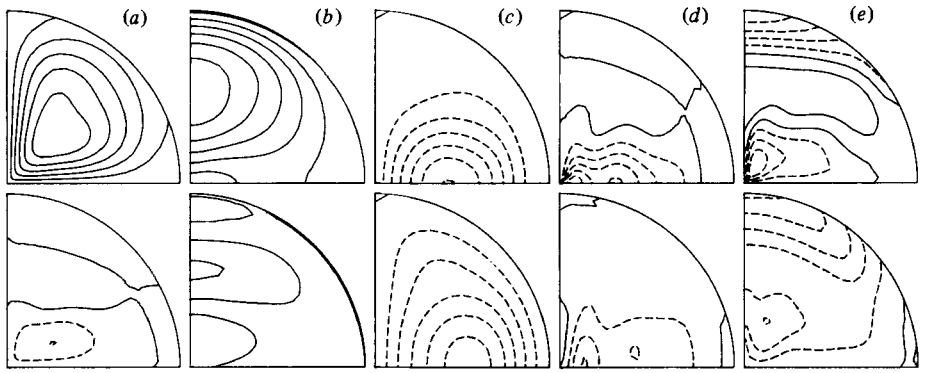

FIGURE 5. As figure 1 but for the field (3.7), $\Lambda = 10$, $m = 1$, $q = 10^{-6}$, dipole parity and $N = L = 20$, giving $R_c = -129{\cdot}2$, $\omega_c = -4{\cdot}530q$. This is an example of the buoyancy-catalysed instability. The contour intervals are (*a*) 1·0, (*b*) 4·0, (*c*) 0·7, (*d*) 100, (*e*) 100.

$0 < m^2 < 4 + (2s/F)\,dF/ds$. For the field (3.7) we found instability at negative values of R for both $m = 1$ and $m = 2$ (see figure 2). The convergence of selected modes ($m = 1$, dipole parity, $\Lambda = 10$) was checked and found to be convincing, and a typical eigenfunction is illustrated in figure 5. There is also some evidence for instability at higher values of m. The local analysis of appendix A is unable to make any predictions about the global stability of (3.7) because locally the field is stable in part of the sphere and unstable in the remainder. The size of the locally unstable region becomes smaller for higher values of m, so it seems likely that if unstable modes do exist for higher values of m they may be localized. The resulting short lengthscale of the instability could not be resolved by the present numerical scheme, so the existence of buoyancy-catalysed instabilities at large values of m is uncertain.

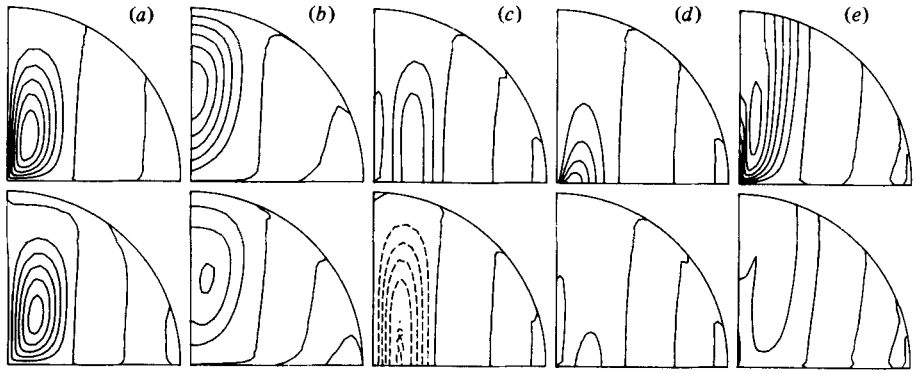

FIGURE 6. As figure 1 but for the field (3.7), $R = 0$, $m = 1$, $q = 10^{-6}$, dipole parity and $N = L = 20$, giving $\Lambda_c = 0{\cdot}9565$, $\omega_c = -343{\cdot}7$. This is an example of the field-gradient instability. The contour intervals are (*a*) 400, (*b*) 2000, (*c*), $100q$, (*d*) 300000, (*e*) 200000.

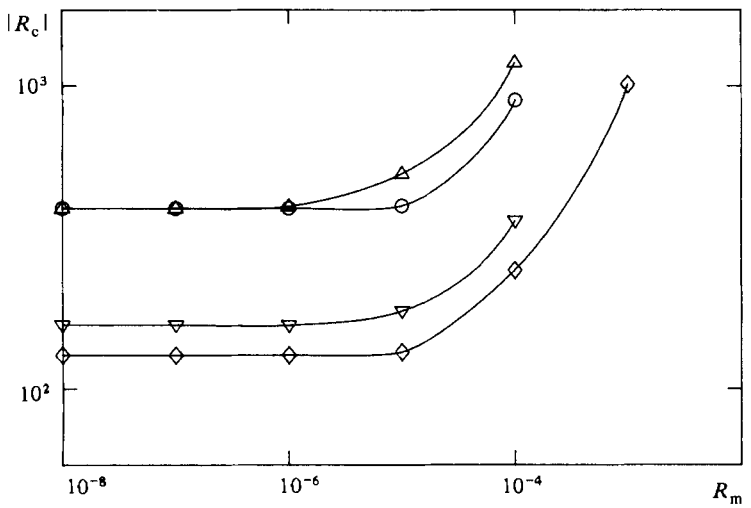

FIGURE 7. The behaviour of the critical Rayleigh number R_c as a shear flow is introduced and its strength R_m is increased. The cases illustrated are for the magnetic field (3.7) and: (*a*) ○, flow (3.11), $\Lambda = 1$, $m = 2$, $q = 10^{-6}$, quadrupole parity, $N = L = 8$; (*b*) △, flow (3.12), $\Lambda = 1$, $m = 2$, $q = 10^{-6}$, quadrupole parity, $N = L = 8$; (*c*) ▽, flow (3.12), $\Lambda = 10$, $m = 1$, $q = 10^{-6}$, dipole parity, $R < 0$, $N = L = 8$; (*d*) ◇, flow (3.12) $\Lambda = 10$, $m = 1$, $q = 10^{-6}$, dipole parity, $R < 0$, $N = L = 20$. The two cases (*c*) and (*d*) show that, although the poor resolution (*c*) may give different quantitative results to the better resolution (*d*), the qualitative behaviour is the same in both cases.

The third mode of instability is also magnetically driven but does not depend on the presence of stratification. Instability occurs when Λ exceeds some critical value, and this mode may be identified as being the magnetic-field gradient instability discussed by Acheson (1973, 1978*a*). This identification is not completely certain, however, because the phase speed found here (see e.g. figure 6) is much larger (by two orders of magnitude) than that predicted by Acheson (see also (A 9)). This disparity can probably be accounted for by the presence of diffusive effects since Acheson's analysis is made in the diffusionless limit ($\Lambda \to \infty$). Here we found Λ_c to be $O(1)$ so diffusive effects must be important and may well be responsible for the size of the phase speed. Convincing convergence was found for the case $m = 1$, dipole

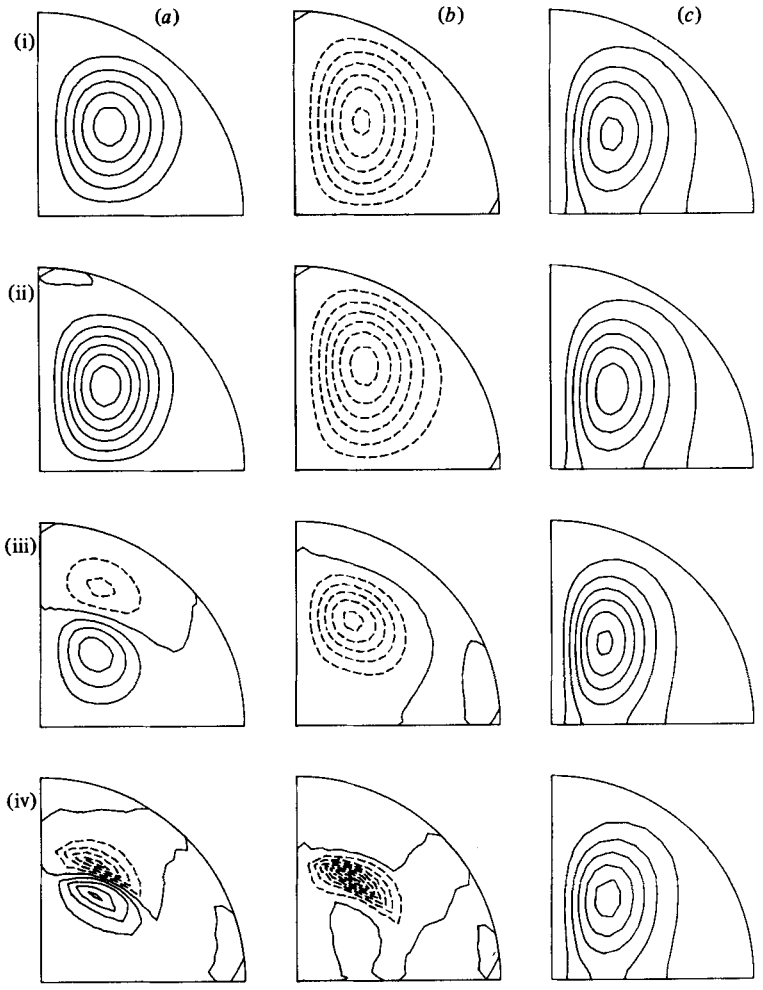

FIGURE 8. The eigenfunction corresponding to case (*a*) of figure 7 is illustrated for (i) $R_m = 0$, (ii) 10^{-5}, (iii) 10^{-4} and (iv) 10^{-3}. For each value of R_m, contour plots of (*a*) $\vartheta^R = \mathrm{Re}\,(\vartheta)$, (*b*) $\vartheta^I = \mathrm{Im}\,(\vartheta)$ and (*c*) $\mathrm{Re}\,(b_r)$ are shown. The latter is changed much less by the shear, and this is also true for the other variables not illustrated. The accuracy of the solution becomes poorer as R_m increases, but the trend is quite distinct; the temperature perturbation becomes increasingly localized. In this case Ω is independent of θ and the localization is about some radius r_L. Both parts of ϑ are shown to illustrate their different behaviour. One part, ϑ^I, has a peak at r_L while the other, ϑ^R, has a zero at r_L with a maximum and minimum on opposite sides. The details of the contour plots are as for figure 1. The contour intervals for (*a*), (*b*) and for (*c*) are: (i), (ii) 0·2, 3·0, (iii) 0·4, 5, (iv) 0·1, 5.

(see figure 6) and the convergence for $m = 3$, dipole looks promising but the eigenfunction is quite detailed and the limit on resolution ($N, L \leqslant 20$) means that we cannot be sure of convergence in this case. The remarks made in reference to the buoyancy-catalysed instability about higher values of m and the local analysis apply equally well to the field-gradient instability.

(*c*) *The effect of differential rotation*

In §3(*b*) we discussed the nature of the shear flow that can be expected in a rapidly rotating magnetic system, and justified studying the stability of the field (3.7) in the absence of any differential rotation. Having done this, we now proceed to investigate

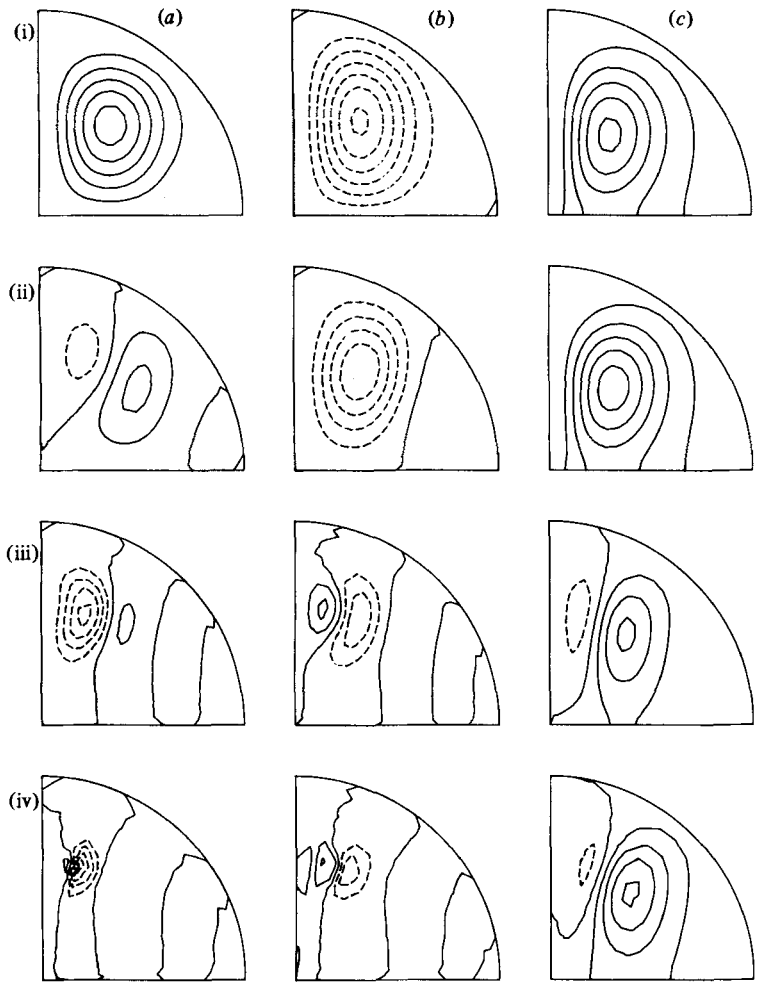

FIGURE 9. As figure 8 but for case (*b*) of figure 7. Here $\Omega = \Omega(r, \theta)$ and ϑ concentrates toward a point (r_L, θ_L). The contour intervals are (i) 0·2, 3·0, (ii) 0·3, 3·0, (iii) 0·5, 7·0, (iv) 0·05, 4.

the effect of differential rotation, and, as discussed in §3(*b*), we have chosen U_0 independently (so it is not necessarily given by $\Omega = \Omega_B + \Omega_T + \Omega_G$). The form of U_0 chosen is

$$U_0 = -\tfrac{25}{16}\sqrt{5}\, r(1-r^2)^2 \sin\theta, \tag{3.11}$$

from Roberts (1972), and we have normalized U_0 such that its maximum modulus is unity. This flow is in the correct sense to draw out poloidal field lines and produce a toroidal field like (3.7) which is directed eastward in the northern hemisphere and westward in the southern hemisphere. There is nothing special about this choice for U_0 (except that Ω is independent of θ) and we believe the results we describe in this section are typical of the effect of differential rotation on convection in a rapidly rotating system. The strength of the differential rotation is measured by the magnetic Reynolds number R_m defined in (2.5) and the effect of shear was investigated by gradually increasing R_m from zero.

The stability of the basic state (3.7), (3.11) was investigated at only a few isolated points in the (Λ, m, q) parameter space because of time and resource limitations. As before, we chose $q = 10^{-6}$ as being a typical representative of $q \ll 1$, and in all cases

we found the following behaviour as the strength R_m of the differential rotation was increased from zero:

(i) the critical Rayleigh number R_c began to increase once R_m became $O(q)$ ($q \ll 1$);

(ii) for $R_m > O(q)$ there is the suggestion that $R_c \propto R_m/q$, but the resolution was not sufficient to establish this relation;†

(iii) the temperature perturbation ϑ becomes increasingly localized at some point (r_L, θ_L) as R_m increases;

(iv) the phase speed of the instability approaches the fluid speed at that point; $\omega_c \to mR_m\Omega(r_L, \theta_L)$.

These features are illustrated in figures 7 and 8. In the case of the flow (3.11), the temperature perturbation becomes localized at a particular radius r_L rather than a point because Ω is independent of θ. Figure 9 illustrates the behaviour for a different flow

$$U_0 = 64r^3(1-r^2)^2 \sin\theta \cos^2\theta. \tag{3.12}$$

It is quite clear that as R_m/q becomes large the resolution that is available becomes completely inadequate to cope with the short lengthscale that develops around (r_L, θ_L). Clearly, to resolve the behaviour properly at large R_m/q, hundreds of grid points are required; a resolution quite unobtainable in the two-dimensional problem we are studying here. It was therefore decided to look at a simpler problem in a plane layer geometry which nevertheless retains the essential physics of the spherical problem. We therefore leave further discussion of the effect of differential rotation to the companion paper (Fearn & Proctor 1983) which solves the plane-layer problem.

4. Summary and concluding remarks

In the preceding sections we discussed the solution of the linear stability problem in a sphere with basic state $\mathbf{B}_0 = B_0(r, \theta)\,\hat{\boldsymbol{\phi}}$ and $\mathbf{U}_0 = U_0(r, \theta)\,\hat{\boldsymbol{\phi}}$. We showed that for $B_0 = s$, $U_0 = 0$ the results obtained here are in agreement with previous work by Fearn (1979*b*). A field (3.7) which is a more realistic representative of the geomagnetic field was then studied and we found little qualitative difference in the behaviour of the thermally driven instabilities compared with $B_0 = s$; the critical Rayleigh number reaches a minimum $O(100)$ when $\Lambda = O(1)$. There were differences, though, when we looked at the magnetically driven instabilities. It was possible to identify two distinct modes: the field-gradient instability of Acheson (1973, 1978*a*), which is essentially independent of stratification, and the buoyancy-catalysed instability, which requires the presence of (stable or unstable) stratification to give the system the freedom to release the magnetic energy. A local stability analysis (appendix A) provides stability criteria (A 11) and (A 15) for these modes. In the case of $B_0 = s$, $U_0 = 0$ the field-gradient instability is absent and the buoyancy-catalysed instability is present only for $m = 1$ (Roberts & Loper 1979; Soward 1979*b*; Fearn 1979*b*); results consistent with the local analysis. In the case of the field (3.7) both field-gradient and buoyancy-catalysed instabilities are present.

Perhaps the most interesting results of the present study were found when we introduced a non-zero shear flow $\mathbf{U}_0$ into the basic state. We concentrated our attention on the thermally driven instability but also investigated the buoyancy-catalysed mode. The behaviour for both is essentially the same; as R_m is increased above $O(q) \ll 1$, the critical Rayleigh number increases, the temperature perturbation becomes localized at some point (r_L, θ_L) and the phase speed of the instability

† This relation may be modified if the angular velocity has a maximum in the interior of the domain (for details see Fearn & Proctor 1983).

approaches the fluid velocity at that point. The instability is thus concentrated at (r_L, θ_L) and is carried around with the flow. The instability has its own intrinsic phase speed with respect to the fluid ($\omega_c \neq 0$ when $R_m = 0$), but this is small compared to the fluid speed when $R_m \gg q$. It is this feature which may have some relevance to the geomagnetic secular variation. The observed drift of the field may represent a combination of the non-axisymmetric part of the field being carried along by the fluid in the core and the phase speed of the wave with respect to the fluid. Depending on the source of the field, both the fluid speed and the phase speed will differ so that the field observed at the surface may represent the net sum of fields generated at different locations and travelling at different speeds. Such a situation need not always result in a westward drift of the field. Indeed there is evidence that in the past the overall drift has been eastward.

A detailed investigation of the effect of the shear flow $\mathbf{U}_0$ has not been possible here because of the limited resolution available. It is however possible to study a similar problem in a plane-layer geometry and find a solution which is separable in s as well as ϕ and t. The ordinary differential equation that remains has again to be solved numerically, but the available resolution in this one-dimensional problem is very much greater than we were able to achieve here. The solution is discussed in the accompanying paper (Fearn & Proctor 1983).

We would like to thank Dr D. J. Acheson, Dr C. A. Jones, Professor P. H. Roberts and Dr A. M. Soward for useful discussions concerning this work and its numerical solution. We are also grateful to the referees of this paper, whose suggestions have led to considerable improvements in its presentation. The inverse iteration program was based on one written by Dr G. O. Roberts. This work was funded by the Science and Engineering Research Council of Great Britain.

Appendix A. Local analysis

A local stability analysis for the basic state $B_0 = B_0(s)$, $U_0 = U_0(s)$ has been made by Acheson (1973, 1978*a*, 1982), and the following criteria for instability were found:

$$\Delta > m^2 \tag{A 1}$$

for the field-gradient instability and

$$\Delta > m^2 - 4 \tag{A 2}$$

for the buoyancy-catalysed instability, where

$$\Delta = \frac{s}{F^2}\frac{dA}{ds}, \quad A = F^2 - \frac{R_m \Omega}{\Lambda}. \tag{A 3}$$

Global analyses have found solutions that are not localized, so we could hardly expect close quantitative agreement between the global and local analyses. However, the local results have proven to be successful in predicting certain qualitative features of the (admittedly rather few) global solutions. Most attention has been given to the case $B_0 = s$, $U_0 = 0$ ($\Delta = 0$) for which the buoyancy-catalysed instability is found to be present (but for $m = 1$ only), while the field-gradient instability is absent (see Soward 1979*b*; Fearn 1979*b*). This is exactly what is predicted by (A 1) and (A 2). It therefore seems worthwhile to extend the local analysis to the more general basic state $B_0(s, z)$, $U_0(s, z)$ in the hope that it will at least guide our numerical solution of the global problem in the right direction. Acheson (1978*b*) has performed this local

analysis, but the context is different and he does not go so far as to derive expressions corresponding to (A 1) and (A 2). This can in fact be done quite simply; before giving the results we briefly sketch how these conditions may be derived from the governing equations presented in §2.

Taking (2.3) with E_η set to zero as our starting point, we make the usual local assumption that the lengthscale of the instability is short compared with the dimensions of the container; that is,

$$\frac{\partial}{\partial s}, \frac{\partial}{\partial z} = O(\epsilon), \quad \epsilon \ll 1, \tag{A 4}$$

but we shall not assume a short azimuthal lengthscale since we are interested in $m = O(1)$. The appropriate scalings for the remaining variables are

$$\frac{\partial}{\partial t} = O(\epsilon^{-2}), \quad \mathbf{u} = O(1), \quad \mathbf{b} = O(\epsilon^2), \quad R_\mathrm{m}, \Lambda = O(\epsilon^{-2}). \tag{A 5}$$

Neglecting all but the leading-order terms and making a modal expansion with all variables proportional to $\exp i(ls+nz)$, the governing equations reduce to a set of linear algebraic equations. After some manipulation, the dependent variables can be eliminated to give

$$(\omega_1 + 2m\Lambda F^2 + ia^2)^2 + m^2\Lambda^2 F^4\left(\Delta - \frac{m^2a^2}{n^2}\right) + m^2\Lambda F^2 qR\left(s - \frac{zl}{n}\right)^2 \frac{\omega_1 + ia^2}{\omega_1 + iqa^2} = 0, \tag{A 6}$$

where

$$\omega_1 = \omega - mR_\mathrm{m}\Omega, \quad a^2 = l^2 + n^2, \tag{A 7}$$

and we have generalized the definition of Δ to be

$$\Delta = \frac{s}{F^2}\left(A_s - \frac{l}{n}A_z\right), \quad A_s = \frac{\partial A}{\partial s}, \quad A_z = \frac{\partial A}{\partial z}. \tag{A 8}$$

The expression (A 6) may also be derived from equation (5.5) of Acheson (1978*b*) by making the necessary modification to convert from the compressible case he considers to the Boussinesq approximation. We now proceed to obtain the instability criteria.

(*a*) *Field-gradient instability*

This instability is essentially independent of stratification and is diffusionless, taking place on a timescale short compared with the magnetic diffusion timescale (see Acheson 1978*a*; Fearn 1979*b*). So setting R and the ia^2 terms in (A 8) to zero we find

$$\omega_1 = -2m\Delta F^2 \pm m\Delta F^2\left(\frac{m^2a^2}{n^2} - \Delta\right)^{\frac{1}{2}}. \tag{A 9}$$

A non-zero growth rate is possible only if

$$\Delta > m^2\left(1 + \frac{l^2}{n^2}\right), \tag{A 10}$$

which may be compared with (A 1), but now the definition (A 8) of Δ (cf. (A 3)) involves l/n, so (A 10) may be optimized over l/n (Acheson 1982 private communication) to give

$$\frac{s}{2F^2}[A_s + (A_s^2 + A_z^2)^{\frac{1}{2}}] > m^2. \tag{A 11}$$

(*b*) *Buoyancy-catalysed instability*

This instability takes place on the thermal diffusion timescale so we must set $\omega_1 = q\omega_2$, and then for simplicity we set $q = 0$ in (A 6) to obtain

$$(2m\Lambda F^2 + ia^2)^2 + m^2\Lambda^2 F^4\left(\Delta - \frac{m^2a^2}{n^2}\right) + m^2\Lambda F^2 R\left(s - \frac{zl}{n}\right)^2 \frac{ia^2}{\omega_2 + ia^2} = 0. \quad \text{(A 12)}$$

This mode is diffusive, so we can demonstrate instability by looking for a marginally stable state. Thus, taking ω_2 to be real, it may be eliminated to give

$$R\left(s - \frac{zl}{n}\right)^2 = C + \frac{16a^4}{m^2 C}, \quad C = \Lambda F^2\left(\frac{m^2a^2}{n^2} - \Delta - 4\right) + \frac{a^4}{m^2\Lambda F^2} \quad \text{(A 13)}$$

The buoyancy-catalysed instability takes place when $R < 0$, so a necessary condition is that

$$\Delta > m^2\left(1 + \frac{l^2}{n^2}\right) - 4, \quad \text{(A 14)}$$

cf. (A 2), or

$$\frac{s}{2F^2}\left[\frac{4F^2}{s} + A_s + \left(\left(\frac{4F^2}{s} + A_s\right)^2 + A_z^2\right)^{\frac{1}{2}}\right] > m^2. \quad \text{(A 15)}$$

(*c*) *Discussion and stability of field* (3.7)

The two criteria (A 11) and (A 15) display two features which may be applicable to global solutions. The first is that (in common with (A 1) and (A 2)) the condition for instability is more difficult to satisfy the greater the azimuthal wavenumber, so we expect larger values of m to be more stable. The second feature displayed by (A 11) and (A 15) is that the presence of any z-structure in the basic state is destabilizing. It is not possible to say much more than this, but it is instructive to see how the instability criteria apply to the field studied numerically in §3.

Substituting (3.7) into (A 11), we find a complicated expression which reduces to $m^2 < s/z$ in the limit $s \gg z$. Clearly, whatever value of m is chosen, this can be satisfied in some region adjacent to the equator. The system is locally unstable in this region but locally stable elsewhere, so the local analysis is unable to predict global instability. It may be that instabilities localized in the unstable region are possible, but these are likely to be damped more strongly by diffusive effects than global instabilities. The numerical scheme used to generate the results of §3 finds the most-unstable mode, so it is unlikely to find localized instabilities. In any case, the resolution of the scheme is good enough only for modes having an $O(1)$ lengthscale.

Appendix B. The numerical scheme

Equations (2.3) are first written in component form with

$$\mathbf{u} = (u_r, u_\theta, u_\phi), \quad \mathbf{b} = (b_r, b_\theta, b_\phi), \quad \text{(B 1)}$$

then (2.3*d*, *e*) and $\hat{\boldsymbol{\phi}}\,.\,(2.3a)$ are used to eliminate u_ϕ, b_ϕ and the pressure p respectively, leaving a system of five equations in u_r, u_θ, b_r, b_θ, and ϑ. We have no boundary condition on u_θ so its radial derivative appearing in $\hat{\mathbf{r}}\,.\,(2.3)$ is removed using $\partial[\hat{\boldsymbol{\theta}}\,.\,(2.3a)]/\partial r$. A further reduction of the system is possible by using $\hat{\boldsymbol{\theta}}\,.\,(2.3a)$ to eliminate u_θ, leaving a set of four coupled partial differential equations in u_r, b_r, b_θ and ϑ. The differential operators are then replaced by second-order finite-difference operators using N grid pints in the r-direction and L in the θ-direction. We shall use

the notation

$$v^{n,l} = v(r = r_n = nh_r,\ \theta = \theta_l = lh_\theta), \tag{B 2}$$

where

$$h_r = 1/N, \quad h_\theta = \pi/2L,$$

and v denotes any of the variables b_r, b_θ, u_r or ϑ.

The boundary condition that $\mathbf{b}$ match to an external potential field $\mathbf{b}^{\mathrm{ex}}$ involves some preliminary calculation. For a given truncation N, L it is necessary to solve for the external field to produce boundary conditions for b_r and b_θ of the form

$$\left.\begin{aligned} b_r^{N,l} &= \sum_{i=1}^{L-1} B_r^{li}(b_r^{N-2,i} - 4b_r^{N-1,i}), \\ b_\theta^{N,l} &= \sum_{i=1}^{L-1} B_\theta^{li}(b_r^{N-2,i} - 4b_r^{N-1,i}), \end{aligned}\right\} \tag{B 3}$$

where $l = 1, \ldots, L-1$ and the boundary-condition matrices $\mathbf{B}_r$ and $\mathbf{B}_\theta$ are calculated using the solution for the external field $\mathbf{b}^{\mathrm{ex}}$ and the condition that $\mathbf{b}$ is continuous at the boundary (see Jepps 1975; Proctor 1975). The remaining boundary conditions can be written in the form

$$u_r^{N,l} = \vartheta^{N,l} = 0, \quad u_r^{0,l} = \vartheta^{0,l} = b_r^{0,l} = b_\theta^{0,l} = 0, \tag{B 4}$$

where again $l = 1, \ldots, L-1$. It is not necessary to perform our numerical solution in the whole region $0 < r < 1$, $0 < \theta < \pi$ provided that the basic state (2.4) satisfies certain symmetry properties about the equator ($\theta = \frac{1}{2}\pi$). We shall assume B_0 to be antisymmetric and U_0 and T_0 to be symmetric,† that is,

$$B_0(r,\theta) = -B_0(r,\pi-\theta), \quad U_0(r,\theta) = U_0(r,\pi-\theta), \quad T_0(r,\theta) = T_0(r,\pi-\theta). \tag{B 5}$$

Then the problem splits into two parities, which we shall call dipole (b_r antisymmetric; b_θ, u_r, ϑ symmetric) and quadrupole (b_r symmetric; b_θ, u_r, ϑ antisymmetric). It is only necessary to compute a solution in the quadrant $0 < r < 1$, $0 < \theta < \frac{1}{2}\pi$ provided that we apply the boundary conditions

$$\left.\begin{aligned} \text{dipole:} \quad & b_r = \frac{\partial b_\theta}{\partial \theta} = \frac{\partial u_r}{\partial \theta} = \frac{\partial \vartheta}{\partial \theta} = 0, \\ \text{quadrupole:} \quad & \frac{\partial b_r}{\partial \theta} = b_\theta = U_r = \vartheta = 0 \end{aligned}\right\} \tag{B 6}$$

at $\theta = \frac{1}{2}\pi$. The boundary conditions are completed by those at $\theta = 0$:

$$\left.\begin{aligned} b_r = \frac{\partial b_\theta}{\partial \theta} = u_r = \vartheta = 0 \quad (m = 1), \\ b_r = b_\theta = u_r = \vartheta = 0 \quad (m > 1). \end{aligned}\right\} \tag{B 7}$$

The problem has now reduced to the solution of a matrix eigenvalue problem of the form

$$\mathbf{A}\mathbf{x} = p\mathbf{B}\mathbf{x}, \tag{B 8}$$

where

$$\left.\begin{aligned} \mathbf{x} &= (\mathbf{v}^{1,1}, \ldots, \mathbf{v}^{1,L-1}, \ldots, \mathbf{v}^{N-1,1}, \ldots, \mathbf{v}^{N-1,L-1}), \\ \mathbf{v}^{i,j} &= (u_r^{i,j}, b_r^{i,j}, b_\theta^{i,j}, \vartheta^{i,j}). \end{aligned}\right\} \tag{B 9}$$

Two methods of solving (B 8) were used. The first is the LR algorithm (Peters & Wilkinson 1971*a*), which was used to find all $3(N-1)(L-1)$ complex eigenvalues

† We consider one exception to this, the checking case $B_0 = r\sin\theta$, $U_0 = 0$. The appropriate changes are to reverse the parities of u_r and ϑ in (B 6).

of the above system with the variable u_r eliminated. (The system then reduces to the form $\mathbf{C}\mathbf{y} = p\mathbf{y}$). The maximum storage available limited N and L to 8 or less, but, since every eigenvalue was found, we could be reasonably sure that we were looking at the most-unstable mode. When a mode has been found approximately using LR, it can be determined to much greater accuracy using the method of inverse iteration (see e.g. Peters & Wilkinson 1971*b*), which finds just one eigenvalue and the corresponding eigenvector. The matrix $\mathbf{A}$ in (B 8) is banded with width $12L-8$, and the method of inverse iteration can take advantage of this to reduce storage and time requirements. Storage for LR is

$$\sim 16[3(N-1)(L-1)]^2,$$

while that for II is

$$\sim 16[4(N-1)(L-1)(12L-8)]$$

so for $N = L \geqslant 6$ there is a saving using II. Further reductions in storage can be made by dividing $\mathbf{A}$ into blocks and dealing with one block at a time in core, the remainder being stored on disc. Though this takes extra time (reading and writing to disc being slow) it enables the resolution to be increased to $N = L = 20$. In fact, time, rather than storage, constraints prevented us from using greater resolution.

REFERENCES

Acheson, D. J. 1973 Hydromagnetic wavelike instabilities in a rapidly rotating stratified fluid. *J. Fluid Mech.* **61**, 609–624.

Acheson, D. J. 1978*a* Magnetohydrodynamic waves and instabilities in rotating fluids. In *Rotating Fluids in Geophysics* (ed. P. H. Roberts & A. M. Soward), pp. 315–349. Academic.

Acheson, D. J. 1978*b* On the instability of toroidal magnetic fields and differential rotation in stars. *Phil. Trans. R. Soc. Lond.* A **289**, 459–500.

Acheson, D. J. 1980 Stable density stratification as a catalyst for instability. *J. Fluid Mech.* **96**, 723–733.

Acheson, D. J. 1982 Thermally convective and magnetohydrodynamic instabilities of a rotating fluid – I. Unpublished manuscript.

Acheson, D. J. & Hide, R. 1973 Hydromagnetics of rotating fluids. *Rep. Prog. Phys.* **36**, 159–221.

Braginsky, S. I. 1980 Magnetic waves in the core of the Earth – II. *Geophys. Astrophys. Fluid Dyn.* **14**, 189–208.

Busse, F. H. & Hood, L. L. 1982 Differential rotation driven by convection in a rapidly rotating annulus. *Geophys. Astrophys. Fluid Dyn.* **21**, 59–74.

Chandrasekhar, S. 1961 *Hydrodynamic and Hydromagnetic Stability.* Clarendon.

Eltayeb, I. A. 1972 Hydromagnetic convection in a rapidly rotating fluid layer. *Proc. R. Soc. Lond.* A **326**, 229–254.

Eltayeb, I. A. 1975 Overstable hydromagnetic convection in a rotating fluid layer. *J. Fluid Mech.* **71**, 161–179.

Eltayeb, I. A. 1981 Propagation and stability of wave motions in rotating magnetic systems. *Phys. Earth Planet. Interiors* **24**, 259–271.

Eltayeb, I. A. & Kumar 1977 Hydromagnetic convective instability of a rotating, self-gravitating fluid sphere containing a uniform distribution of heat sources. *Proc. R. Soc. Lond.* A **353**, 145–162.

Eltayeb, I. A. & Roberts, P. H. 1970 On the hydromagnetics of rotating fluids. *Astrophys. J.* **162,** 699–701.

Fearn, D. R. 1979 *a* Thermally driven hydromagnetic convection in a rapidly rotating sphere. *Proc. R. Soc. Lond.* A **369**, 227–242.

Fearn, D. R. 1979*b* Thermal and magnetic instabilities in a rapidly rotating fluid sphere. *Geophys. Astrophys. Fluid Dyn.* **14**, 103–126.

Fearn, D. R. & Loper, D. E. 1981 Compositional convection and stratification of Earth's core. *Nature* **289**, 393–394.

FEARN, D. R. & PROCTOR, M. R. E. 1983 The stabilizing role of differential rotation on hydromagnetic waves. *J. Fluid Mech.* **128**, 21–36.

GUBBINS, D., MASTERS, T. G. & JACOBS, J. A. 1979 Thermal evolution of the Earth's core. *Geophys. J. R. Astr. Soc.* **59**, 57–99.

JEPPS, S. A. 1975 Numerical models of hydromagnetic dynamos. *J. Fluid Mech.* **67**, 625–646.

LOPER, D. E. & ROBERTS, P. H. 1983 Compositional convection and the gravitationally powered dynamo. In *Stellar and Planetary Magnetism* (ed. A. M. Soward). Gordon & Breach.

MALKUS, W. V. R. 1967 Hydromagnetic planetary waves. *J. Fluid Mech.* **28**, 793–802.

MOFFATT, H. K. 1978 *Magnetic Field Generation in Electrically Conducting Fluids*. Cambridge University Press.

PETERS, G. & WILKINSON, J. H. 1971*a* Eigenvectors of real and complex matrices by *LR* and *QR* triangularisations. In *Handbook for Automatic Computation*, vol. 2: *Linear Algebra* (ed. J. H. Wilkinson & C. Reinsch), pp. 370–395. Springer.

PETERS, G. & WILKINSON, J. H. 1971*b* The calculation of specified eigenvectors by inverse iteration. In *Handbook for Automatic Computation*, vol. 2: *Linear Algebra* (ed. J. H. Wilkinson & C. Reinsch), pp. 418–439. Springer.

PROCTOR, M. R. E. 1975 Non-linear mean field dynamo models and related topics. Ph.D. thesis, University of Cambridge.

ROBERTS, P. H. 1968 On the thermal instability of a rotating-fluid sphere containing heat sources. *Phil. Trans. R. Soc. London.* A **263**, 93–117.

ROBERTS, P. H. 1972 Kinematic dynamo models. *Phil. Trans. R. Soc. Lond.* A **272**, 663–703.

ROBERTS, P. H. 1978 Magneto-convection in a rapidly rotating fluid. In *Rotating Fluids in Geophysics* (ed. P. H. Roberts & A. M. Soward), pp. 421–435. Academic.

ROBERTS, P. H. & LOPER, D. E. 1979 On the diffusive instability of some simple steady magnetohydrodynamic flows. *J. Fluid Mech.* **90**, 641–668.

SOWARD, A. M. 1977 On the finite amplitude thermal instability of a rapidly rotating fluid sphere. *Geophys. Astrophys. Fluid Dyn.* **9**, 19–74.

SOWARD, A. M. 1979*a* Convection driven dynamos. *Phys. Earth Planet. Interiors* **20**, 134–151.

SOWARD, A. M. 1979*b* Thermal and magnetically driven convection in a rapidly rotating fluid layer. *J. Fluid Mech.* **90**, 669–684.

WHALER, K. A. 1980 Does the whole of the Earth's core convect? *Nature* **287**, 528–530.